

Fracture Network Mathematics

Daniel S. Brox

Independent Researcher, Vancouver, Canada

Email: danbrox@gmail.com

How to cite this paper: Brox, D.S. (2026)
Fracture Network Mathematics. *Journal of
Modern Physics*, 17, 111-123.
<https://doi.org/10.4236/jmp.2026.172007>

Received: December 3, 2025

Accepted: February 3, 2026

Published: February 6, 2026

Copyright © 2026 by author(s) and
Scientific Research Publishing Inc.
This work is licensed under the Creative
Commons Attribution International
License (CC BY 4.0).

<http://creativecommons.org/licenses/by/4.0/>



Open Access

Abstract

Analytic solutions for elastostatic displacement due to vertical/shear traction applied to the faces of a single crack in a 2D plane are reviewed in Section 2. The purpose of this review is to introduce mathematics relevant to specifying multi-crack elastostatic displacements. In Section 3, the relation between multi-crack elastostatic displacement fields and Riemann surface geometry is discussed. Section 4 explains why 2D multi-crack solutions appear limited to describe idealized cracks in 2 spatial dimensions, and conjectures how 3D fracture networks in the lithosphere can be described in terms of singular spectrum analysis of crack phase fields.

Keywords

Mode I, Mode II, Multi-Crack, Statistics, Singular Spectrum Analysis

1. Introduction

Analytic solutions for elastostatic displacement due to vertical/shear traction applied to the faces of a single crack in a 2D plane are reviewed in Section 2. The purpose of this review is to introduce mathematics relevant to specifying multi-crack elastostatic displacements. In Section 3, the relation between multi-crack elastostatic displacement fields and Riemann surface geometry is discussed. Section 4 explains why 2D multi-crack solutions appear limited to describing idealized cracks in 2 spatial dimensions, and conjectures how 3D fracture networks in the lithosphere can be described in terms of singular spectrum analysis of crack phase fields.

2. Single Crack 2D Elastostatic Displacement

2.1. Yoffe Mode I Crack

Consider a sharp crack of length R propagating with constant velocity v in a uniform elastic material in 2D plane strain conditions, whereby the crack tips are located at $(vt - R, 0)$ and $(vt, 0)$. In terms of coordinates $(\xi, y) = (x - vt, y)$ in

which the crack tips are fixed at $(-R, 0)$ and $(0, 0)$, the elastic displacement $\mathbf{u}(x, y, t)$ can be expressed in terms of scalar and vector potentials $\phi(\xi, y)$ and $\vec{\psi} = (0, 0, \psi(\xi, y))$ as:

$$\mathbf{u}(x, y, t) = \nabla\phi + \nabla \times \vec{\psi}, \tag{1}$$

where:

$$\alpha_p^2 \frac{\partial^2 \phi}{\partial \xi^2} + \frac{\partial^2 \phi}{\partial y^2} = 0, \tag{2}$$

$$\alpha_s^2 \frac{\partial^2 \psi}{\partial \xi^2} + \frac{\partial^2 \psi}{\partial y^2} = 0, \tag{3}$$

for constants $\alpha_p = \sqrt{1 - v^2/v_p^2}$ and $\alpha_s = \sqrt{1 - v^2/v_s^2}$ specified by v and the P and SV wave velocities v_p and v_s [1]. In turn, the potentials $\phi(\xi, y)$ and $\psi(\xi, y)$ can be expressed in terms of analytic functions $F(\zeta)$ and $G(\zeta)$ as:

$$\phi(\xi, y) = \text{Re } F(\zeta_p), \tag{4}$$

$$\psi(\xi, y) = \text{Im } G(\zeta_s), \tag{5}$$

for $\zeta_p = \xi + i\alpha_p y$ and $\zeta_s = \xi + i\alpha_s y$, whereby elastic displacement field and stress field components are given by the equations:

$$u_x(x, y, t) = \text{Re}(F'(\zeta_p) + \alpha_s G'(\zeta_s)), \tag{6}$$

$$u_y(x, y, t) = -\text{Im}(\alpha_p F'(\zeta_p) + G'(\zeta_s)), \tag{7}$$

$$\sigma_{xx}(x, y, t) = \text{Re}\left((\lambda + 2\mu - \lambda\alpha_p^2)F''(\zeta_p) + 2\mu\alpha_s G''(\zeta_s)\right), \tag{8}$$

$$\sigma_{yy}(x, y, t) = -\mu \text{Re}\left((1 + \alpha_s^2)F''(\zeta_p) + 2\alpha_s G''(\zeta_s)\right), \tag{9}$$

$$\sigma_{xy}(x, y, t) = -\mu \text{Im}\left(2\alpha_p F''(\zeta_p) + (1 + \alpha_s^2)G''(\zeta_s)\right), \tag{10}$$

for Lamé parameters λ and μ .

Now assume the crack is Mode I, in which a uniform vertical traction σ_p acts on the crack faces while the shear traction applied to the crack faces is 0, as illustrated in **Figure 1**-left. In this case, the $-R < \xi < 0$ crack face boundary conditions are:

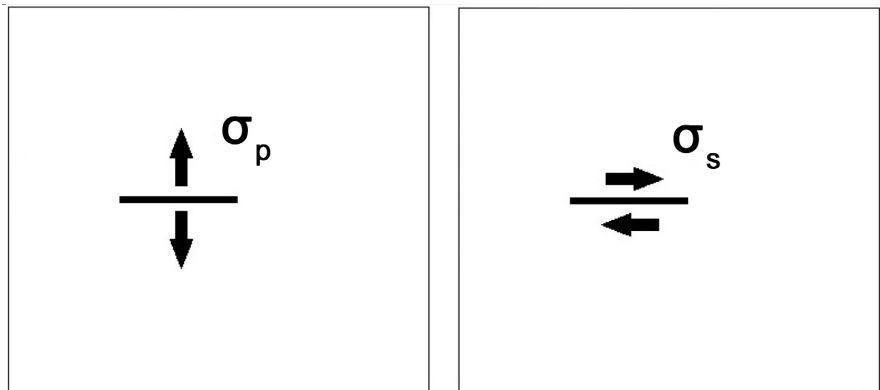


Figure 1. Stationary Yoffe Mode I crack (left) and Rice Mode II crack (right).

$$\sigma_{yy}(\xi, 0^\pm) = -\sigma_p, \quad (11)$$

$$\sigma_{xy}(\xi, 0^\pm) = 0. \quad (12)$$

and the potentials $\phi(\xi, y)$ and $\psi(\xi, y)$ have the symmetries $\phi(\xi, -y) = \phi(\xi, y)$ and $\psi(\xi, -y) = -\psi(\xi, y)$ imply $u_x(x, -y, t) = u_x(x, y, t)$ and $u_y(x, -y, t) = -u_y(x, y, t)$, in keeping with x-axis reflection symmetry of a Mode I crack displacement solution. Furthermore, the Cauchy-Riemann equations imply $F(\bar{\zeta}) = \overline{F(\zeta)}$ and $G(\bar{\zeta}) = \overline{G(\zeta)}$.

The symmetries of F and G , together with Equations (10) and (12), imply the function:

$$E(\zeta) = 2\alpha_p F''(\zeta) + (1 + \alpha_s^2) G''(\zeta), \quad (13)$$

is continuous across the crack line between $\zeta = -R$ and $\zeta = 0$, and is therefore entire. Given that the elastic velocity and stress fields are zero at points remote from the crack, Liouville's theorem on bounded entire functions implies:

$$G''(\zeta) = -\frac{2\alpha_p}{1 + \alpha_s^2} F''(\zeta). \quad (14)$$

Equations (9) and (14) together with condition (11) imply:

$$\operatorname{Re} F''(\xi) = -\frac{1 + \alpha_s^2}{D} \frac{\sigma_p}{\mu}, \quad -R < \xi < 0, \quad (15)$$

where $D = 4\alpha_p \alpha_s - (1 + \alpha_s^2)^2$, and discontinuity of $\operatorname{Im} F''(\zeta)$ across the crack line occurs as necessary to account for discontinuity in elastic displacement. Assuming $\sqrt{\zeta(\zeta + R)}$ is defined as a single valued function on the complex plane with a branch cut between $\zeta = -R$ and $\zeta = 0$ along $y = 0$, the function:

$$\left(F''(\zeta) + \frac{1 + \alpha_s^2}{D} \frac{\sigma_p}{\mu} \right) \sqrt{\zeta(\zeta + R)} - \frac{1 + \alpha_s^2}{D} \frac{\sigma_p}{\mu} (\zeta + R/2), \quad (16)$$

is continuous across the crack line, and is therefore an entire function that approaches 0 as $|\zeta| \rightarrow \infty$, implying:

$$F''(\zeta) = \frac{1 + \alpha_s^2}{D} \frac{\sigma_p}{\mu} \left(\frac{\zeta + R/2}{\sqrt{\zeta(\zeta + R)}} - 1 \right), \quad (17)$$

and:

$$G''(\zeta) = -\frac{2\alpha_p}{D} \frac{\sigma_p}{\mu} \left(\frac{\zeta + R/2}{\sqrt{\zeta(\zeta + R)}} - 1 \right). \quad (18)$$

Equations (17) and (18) imply the normal stress distribution $\sigma_{yy}(\xi, 0)$ on the crack line ahead of the advancing crack tip is:

$$\sigma_{yy}(\xi, 0) = \sigma_p \left(\frac{\xi + R/2}{\sqrt{\xi(\xi + R)}} - 1 \right), \quad \xi > 0. \quad (19)$$

Integration of Equations (17) and (18) gives equations:

$$F'(\zeta) = \frac{1 + \alpha_s^2}{D} \frac{\sigma_p}{\mu} \left(\sqrt{\zeta(\zeta + R)} - \zeta - R/2 \right), \quad (20)$$

and:

$$G'(\zeta) = -\frac{2\alpha_p \sigma_p}{D \mu} \left(\sqrt{\zeta(\zeta + R)} - \zeta - R/2 \right). \tag{21}$$

in which constants of integration have been selected so elastic displacements are 0 at remote points. Assuming $\sqrt{\zeta(\zeta + R)}$ is defined as a single valued function on the complex plane with a branch cut between $\zeta = -R$ and $\zeta = 0$ along $y = 0$, Equations (20) and (21) together with Equation (7) imply the crack opening displacement is:

$$u_y(\xi, 0^+) = \frac{\alpha_p v^2 \sigma_p}{D v_s^2 \mu} \sqrt{-\xi(\xi + R)}, \quad -R < \xi < 0. \tag{22}$$

2.2. Rice Mode II Crack

Now assume the crack is Mode II, in that a uniform shear traction σ_s is applied to the crack faces while the vertical traction applied to the crack faces is 0, as illustrated in **Figure 1**-right [2]. In this case the $-R < \xi < 0$ crack face boundary conditions are:

$$\sigma_{xy}(\xi, 0^\pm) = -\sigma_s, \tag{23}$$

$$\sigma_{yy}(\xi, 0^\pm) = 0, \tag{24}$$

and the potentials $\phi(\xi, y)$ and $\psi(\xi, y)$ have the symmetries $\phi(\xi, -y) = -\phi(\xi, y)$ and $\psi(\xi, -y) = \psi(\xi, y)$ so that:

$$u_x(x, -y, t) = -u_x(x, y, t), \tag{25}$$

$$u_y(x, -y, t) = u_y(x, y, t), \tag{26}$$

and:

$$F(\bar{\zeta}) = -\overline{F(\zeta)}, \tag{27}$$

$$G(\bar{\zeta}) = -\overline{G(\zeta)}, \tag{28}$$

as necessary to satisfy the Cauchy-Riemann equations for analytic functions $F(\zeta)$ and $G(\zeta)$.

Equations (27) and (28) imply the function:

$$E(\zeta) = -(1 + \alpha_s^2) F''(\zeta) - 2\alpha_s G''(\zeta), \tag{29}$$

is continuous across the crack line, and therefore entire. Furthermore, vanishing of stress and velocity field displacements as $|\zeta| \rightarrow \infty$ imply $E(\zeta)$ is bounded at infinity, and thus identically 0 by Liouville's theorem. Consequently:

$$G''(\zeta) = -\frac{1 + \alpha_s^2}{2\alpha_s} F''(\zeta), \tag{30}$$

which together with boundary condition (23) implies that along the crack line:

$$Im F''(\xi) = \frac{2\alpha_s \sigma_s}{D \mu}, \quad -R < \xi < 0, \tag{31}$$

where $D = 4\alpha_p\alpha_s - (1 + \alpha_s^2)^2$, and discontinuity of $Re F''(\zeta)$ across the crack line occurs as necessary to account for discontinuity in elastic displacement. Assuming $\sqrt{\zeta(\zeta + R)}$ is defined as a single valued function on the complex plane with a branch cut between $\zeta = -R$ and $\zeta = 0$ along $y = 0$, the function:

$$\left(F''(\zeta) - \frac{2i\alpha_s \sigma_s}{D \mu} \right) \sqrt{\zeta(\zeta + R)} + \frac{2i\alpha_s \sigma_s}{D \mu} (\zeta + R/2), \quad (32)$$

is continuous across the crack line, and is therefore an entire function that approaches 0 as $|\zeta| \rightarrow \infty$, implying:

$$F''(\zeta) = -\frac{2i\alpha_s \sigma_s}{D \mu} \left(\frac{\zeta + R/2}{\sqrt{\zeta(\zeta + R)}} - 1 \right), \quad (33)$$

and:

$$G''(\zeta) = \frac{i(1 + \alpha_s^2) \sigma_s}{D \mu} \left(\frac{\zeta + R/2}{\sqrt{\zeta(\zeta + R)}} - 1 \right). \quad (34)$$

Integration of Equations (33) and (34) gives equations:

$$F'(\zeta) = -\frac{2i\alpha_s \sigma_s}{D \mu} \left(\sqrt{\zeta(\zeta + R)} - \zeta - R/2 \right), \quad (35)$$

and:

$$G'(\zeta) = \frac{i(1 + \alpha_s^2) \sigma_s}{D \mu} \left(\sqrt{\zeta(\zeta + R)} - \zeta - R/2 \right), \quad (36)$$

in which constants of integration have been selected so elastic displacements are 0 at remote points. Assuming $\sqrt{\zeta(\zeta + R)}$ is defined as a single valued function on the complex plane with a branch cut between $\zeta = -R$ and $\zeta = 0$ along $y = 0$, Equations (35) and (36) together with Equation (6) imply the crack opening displacement is:

$$u_x(\xi, 0^+) = \frac{\alpha_s v^2 \sigma_s}{D v_s^2 \mu} \sqrt{-\xi(\xi + R)}, \quad -R < \xi < 0. \quad (37)$$

3. Multi-Crack 2D Elastostatic Displacement

3.1. Crack Geometry: Hyperelliptic Curves

For the purpose of calculating multi-crack 2D elastostatic displacements, cracks will be identified with branch cuts of the complex plane specifying sheets of Riemann surfaces. To explain this statement in detail, consider the equation:

$$Y^2 = (X - b_1)(X - b_2) \cdots (X - b_{2g+1})(X - b_{2g+2}), \quad (38)$$

relating complex variables Y and ζ with $2g + 2$ different complex values b_i . For each pair of values (b_{2i-1}, b_{2i}) the expression:

$$\sqrt{(X - b_{2i-1})(X - b_{2i})}, \quad (39)$$

can be a single valued analytic function on the complex X -plane with a branch cut joining the points b_{2i-1} and b_{2i} , and this function is unique up to choice of sign. Iterating selection of a branch for square root for $1 \leq i \leq g+1$, it the product:

$$Y = \sqrt{(X - b_1)(X - b_2) \cdots (X - b_{2g+1})(X - b_{2g+2})}, \tag{40}$$

can be defined as a single valued analytic function on the complex X -plane, up to choice of sign, away from a finite set of branch cuts joining branch points b_{2i-1} and b_{2i} in pairs. For this reason, the projection:

$$(X, Y) \rightarrow X, \tag{41}$$

from points satisfying Equation (38) to the complex X -plane is a double cover of the complex plane away from the branch cuts.

The projective completion of non-compact hyperelliptic curve (38) is the compact hyperelliptic curve:

$$Y^2 Z^{2g} = (X - b_1 Z)(X - b_2 Z) \cdots (X - b_{2g+1} Z)(X - b_{2g+2} Z), \tag{42}$$

in $\mathbb{C}P^2$. From this point of view, the projection:

$$(X : Y : Z) \rightarrow (X : Z), \tag{43}$$

from points on curve (42) to the Riemann sphere $\mathbb{C}P^1$ is a double cover with branch points at $X/Z = b_i$. When $|X/Z| \gg \max |b_i|$, Equation (42) implies:

$$\left(\frac{Y}{Z}\right)^2 \approx \left(\frac{X}{Z}\right)^{2g+2}, \tag{44}$$

so the point $(X : Z)$ with $Z \neq 0$ is covered by the two points $(X : \pm X^{g+1}/Z^g : Z)$. Therefore, for $g=0$ the point at infinity $(1:0)$ is double covered by $(1:1:0)$ and $(1:-1:0)$ while for $g \geq 1$ the point at infinity $(1:0)$ is double covered by $(0:1:0)$. With resolution of the $g \geq 1$ singularity at $(X : Y : Z) = (0, 1, 0)$, projection (43) can be drawn as a projection from a non-singular genus g Riemann surface to the Riemann sphere as shown in **Figure 2**. In this image, the inverse image of each branch cut is shown as a closed loop on the surface.

3.2. Elastostatic Displacement: Differential Forms

For a superposition of vertical/shear traction acting on the crack faces, the Mode I and Mode II single crack elastostatic displacement potentials ϕ and ψ independently solve the 2D Laplace equation:

$$\frac{\partial^2 \phi}{\partial \xi^2} + \frac{\partial^2 \phi}{\partial y_p^2} = 0, \tag{45}$$

$$\frac{\partial^2 \psi}{\partial \xi^2} + \frac{\partial^2 \psi}{\partial y_s^2} = 0, \tag{46}$$

away from the crack lines in the $(\xi, y_p) = (\xi, \alpha_p y)$ and $(\xi, y_s) = (\xi, \alpha_s y)$

planes. By Gauss' and Stokes' theorems, the line integrals:

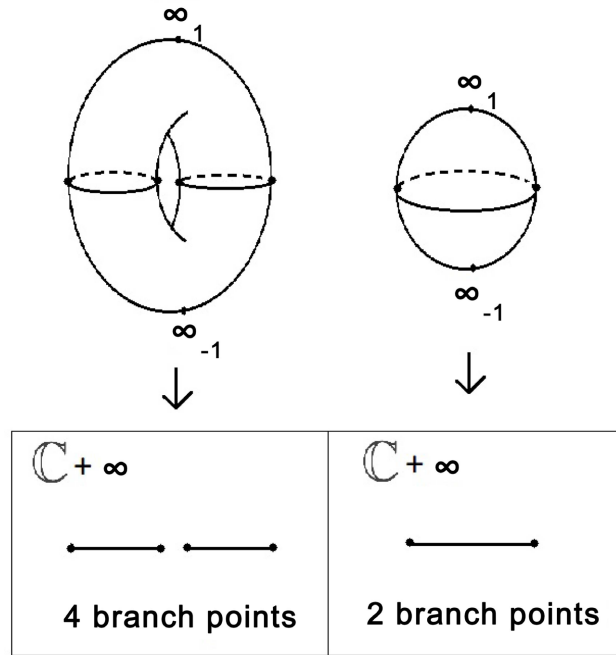


Figure 2. Double cover of Riemann sphere ($\mathbb{C} + \infty$) by genus 1 and genus 0 hyperelliptic curves with 4 and 2 branch points.

$$\oint_{C_p} \mathbf{u} \cdot \mathbf{n} ds = \oint_{C_p} \nabla \phi \cdot \mathbf{n} ds = \text{Im} \left(\oint_{C_p} F'(\zeta_p) d\zeta_p \right) = \frac{\pi \alpha_p v^2 R^2}{4 D v_s^2 \mu} \sigma_p, \quad (47)$$

and:

$$\oint_{C_s} \mathbf{u} \cdot \mathbf{t} ds = \oint_{C_s} (\nabla \times \vec{\psi}) \cdot \mathbf{t} ds = \text{Re} \left(\oint_{C_s} G'(\zeta_s) d\zeta_s \right) = -\frac{\pi \alpha_s v^2 R^2}{4 D v_s^2 \mu} \sigma_s, \quad (48)$$

each obtain a constant value for any closed contours C_p and C_s encircling the crack once counterclockwise in the ζ_p and ζ_s planes. Moreover, these constant values can be non-zero because the analytic functions $F(\zeta)$ and $G(\zeta)$ are multi-valued, as may be anticipated based on $1/|\zeta|$ dependence of elastic displacement at points remote from the cracks. This dependence can be extracted from singular behavior of differential forms $F'(\zeta)d\zeta$ and $G'(\zeta)d\zeta$ at infinity evaluated using the substitution $\bar{\zeta} = 1/\zeta$. Noting that:

$$\sqrt{\zeta(\zeta + R)} - \zeta - R/2 = -\frac{R^2/4}{\sqrt{\zeta(\zeta + R)} + \zeta + R/2} \propto \bar{\zeta}, \quad (49)$$

for $|\zeta| \gg R$, and $d\zeta = -d\bar{\zeta}/\bar{\zeta}^2$, it is evident that both $F'(\zeta)d\zeta$ and $G'(\zeta)d\zeta$ have a simple pole at infinity. For this reason, the integral of the pull-back of either form to a Riemann sphere around the closed contour shown in **Figure 2** is non-zero, because the form has a simple pole on both the inside and outside of the contour.

For $g \geq 1$, $g+1$ cracks in the ζ_p or ζ_s plane can be viewed as branch

cuts for a double cover of the plane by a hyperelliptic curve of genus g , and multi-crack elastostatic displacement solutions for constant vertical or shear surface tractions are associated with meromorphic 1-forms on the curve. The Riemann-Roch theorem applies to calculate the dimension of the complex vector space V_ω of meromorphic 1-forms ω on a non-singular Riemann surface of genus g with simple poles at 2 prescribed points as being $g+1$. More specifically, the theorem for curves states that if \mathcal{K} is a canonical divisor on a non-singular Riemann surface of genus g , then:

$$\begin{aligned} \dim_{\mathbb{C}} V_\omega &= l(\mathcal{K} + \infty_1 + \infty_{-1}) \\ &= g - 1 + l(-\infty_1 - \infty_{-1}) - \deg(-\infty_1 - \infty_{-1}) \\ &= g - 1 + 0 - (-2) \\ &= g + 1. \end{aligned} \tag{50}$$

where $l(D)$ is the complex dimension of the vector space of meromorphic functions on the Riemann surface bounded by divisor D [3]. Consequently, if an elastostatic displacement vector field \mathbf{u} in the multi-cracked $(x - vt, y)$ plane is associated with meromorphic 1-forms $F'(\zeta_p)d\zeta_p$ and $G'(\zeta_s)d\zeta_s$ in the ζ_p and ζ_s planes via Helmholtz decomposition (1) and Equations (4) and (5), the pullback of either 1-form to a non-singular genus g Riemann surface can each be expressed as a linear combination of a basis $\omega_1, \omega_2, \dots, \omega_g, \omega_\infty$ for a vector space of meromorphic 1-forms V_ω on the respective curve, where each ω_i is holomorphic and ω_∞ has simple poles at the points $\infty_{\pm 1}$. When $v = 0$, the ζ_p and ζ_s planes coincide and both meromorphic 1-forms $F'(\zeta_p)d\zeta_p$ and $G'(\zeta_s)d\zeta_s$ pullback to 1-forms on the same Riemann surface. In this case, the complex dimension $g+1$ is in agreement with the fact that there are $2g+2$ real parameters $\sigma_{p,i}$ and $\sigma_{s,i}$ available to specify constant vertical and shear surface tractions on crack faces of the multi-crack system, since the elastostatic displacement fields \mathbf{u} associated with sets of constant surface tractions form a real vector space.

4. 3D Fracture Networks

Correspondence between 2D multi-crack configurations with hyperelliptic curves suggests a change in 2D crack configuration (e.g. crack growth) may be modeled as a change in the shape of a Riemann surface. This fact is of scientific interest because current methods of modeling and simulating crack growth invoke empirical time evolution equations for crack phase fields (*i.e.* damage fields), and these methods may be advanced by more systematic time evolution modeling [4]. However, practical application of the multi-crack Riemann surface model to modeling crack growth in laboratory rock samples and the lithosphere appears lacking for at least two reasons:

- It is not clear how the 2D Riemann surface model can be generalized to describe cracks of arbitrary orientation and finite width in 3 spatial dimensions.
- It is not clear how the 2D Riemann surface model can be generalized to de-

scribe elastostatic displacement of a material whose elastic parameters vary in space and time.

To address these problems, an introductory discussion of 3D fracture in laboratory rock samples and the lithosphere is presented, and 3D fracture network dynamics preceding an earthquake are characterized in terms of singular spectrum analysis of a crack phase field. Physically, specification of a crack phase field in a laboratory rock sample or region of the lithosphere adjusts material elastic parameters based on crack damage, with an increase in the crack phase field at a particular spatial location corresponding to a reduction in elastic shear modulus of material. Within the lithosphere, changes in material shear modulus can be detected as changes in local earthquake coda wave signals on seismograms, allowing for detection of a fault damage zone formed before earthquake fault rupture. Conjecturally, time evolution of the crack phase field preceding an earthquake is governed by a finite dimensional nonlinear dynamical system with phase space dimension equal to a number of dynamic modes of fault damage. From this point of view, it remains possible that the underlying nonlinear dynamical system phase space of a 3D crack phase field is related to the geometry of Riemann surfaces, although more detailed investigation is required to determine whether or not this is the case.

4.1. Laboratory Rock Fracture

Consider a triaxial compression test on a rock sample for which axial compressive strain is applied along principal axis 1 while compressive stresses in the direction of principal axes 2 and 3 are held constant. Assume the initial compressive stresses satisfy $\sigma_1 > \sigma_2 > \sigma_3$, and as σ_1 is increased towards a maximum value $\sigma_{1,\max}$, plastic strain hardening of the rock sample occurs. Also assume that when ϵ_1 is increased beyond the strain $\epsilon_{1,\max}$ at which $\sigma_1 = \sigma_{1,\max}$, strain softening of the rock occurs with formation of a shear band along a plane where the rock ultimately undergoes shear failure. Technically, the constitutive model of the rock may be defined using a Mohr-Coulomb yield criterion with mobilized friction angle/cohesion and a non-associated plastic flow rule [5].

Physically accurate and well defined mathematical description of the rock strain softening regime requires addition of at least two features to the strain hardening non-associated plasticity model:

- Strain rate softening of rock shear strength [6].
- Regularization of rock plastic flow introducing a non-zero shear band width [7].

If it is assumed that with consideration of these technical details, and definition of a finite element mesh, a global elasto-plastic tangent stiffness operator $K_T^{ep}(\tau)$ can be defined for the rock sample throughout triaxial compression at a constant strain rate at each time τ , Newton's equation of motion dictates that the equation:

$$M\ddot{U}(t) + C(\tau)\dot{U}(t) + K_T^{ep}(\tau)U(t) = F(t), \quad (51)$$

describes time evolution of a vector perturbation $U(t)$ to the finite element nodal elasto-plastic displacements at time τ , where M is a lumped mass matrix, $C(\tau)$ is a damping matrix at time τ , and $F(t)$ is a perturbation of the externally applied nodal force vector [8].

4.2. Lithospheric Fracture Networks

Typically, plastic deformation of rock material occurs with cracking (*i.e.* damage). In seismology, earthquake faults are observed to be surrounded by damage zones, and detecting fault damage zone formation by monitoring real time variation of local earthquake coda wave signals on seismograms has been identified as a possible method of predicting earthquakes [9]. According to this method, in a frequency band centered at angular frequency ω , time variation of the local earthquake coda $Q(\omega)$ value at a particular seismic station can be attributed to time variation of the anelastic and/or scattering Q values $Q_i(\omega)$ and $Q_s(\omega)$ according to the equation:

$$\frac{1}{Q(\omega)} = \frac{1}{Q_i(\omega)} + \frac{1}{Q_s(\omega)}, \quad (52)$$

and decrease of $Q_s(\omega)$ in time may reflect earthquake precursor dynamics in the lithosphere. More specifically, based on a single backscattering model of coda wave signals, Q_s scales with signal frequency according to the power law:

$$Q_s(\omega) \propto \omega^{2H}, \quad (53)$$

and may therefore contribute to real time variation of $Q(\omega)$ if the Hurst exponent H changes in time [10]. Fundamentally, the Hurst exponent H is related to the power spectrum of random S-wave velocity model inhomogeneities in the lithosphere $W_{3D}(k)$, where k is wave number, via the relation [11]:

$$W_{3D}(k) \propto k^{-2H-3}. \quad (54)$$

These random inhomogeneities can be attributed to a fracture network superimposed on a fixed seismic velocity model background, such as a 1D layered velocity model, with fracture size statistics characterized by Equation (54).

4.3. Crack Phase Field Singular Spectrum Analysis

Suppose a scalar crack phase field influences Lamé elastic parameters $\lambda(x, y, z, \tau)$ and $\mu(x, y, z, \tau)$ of a 3D laboratory rock sample or lithospheric region via the equations:

$$\lambda(x, y, z, \tau) = \lambda_0(x, y, z) + \lambda_r \phi(x, y, z, \tau) \quad (55)$$

$$\mu(x, y, z, \tau) = \mu_0(x, y, z) + \mu_r \phi(x, y, z, \tau), \quad (56)$$

where $\lambda_0(x, y, z)$ and $\mu_0(x, y, z)$ are the Lamé parameters of uncracked rock at location (x, y, z) , $\phi(x, y, z, \tau)$ is the crack phase field with value 0 for uncracked material and 1 for maximally damaged material, and λ_r and μ_r are constants [12]. If the crack phase field can be directly measured at a particular

3D location P at regular time intervals, the sequence of phase field values $\phi[i] = \phi(P, \tau_0 + (i-1)\Delta\tau)$ can be used to write a trajectory matrix $\mathcal{X}(\phi[i])$:

$$\mathcal{X}(\phi[i]) = \frac{1}{\sqrt{N}} \begin{bmatrix} \phi[1] & \phi[2] & \phi[3] & \cdots & \phi[N] \\ \phi[2] & \phi[3] & \phi[4] & \cdots & \phi[N+1] \\ \vdots & \vdots & \vdots & \ddots & \vdots \\ \phi[N] & \phi[N+1] & \phi[N+2] & \cdots & \phi[N+n-1] \end{bmatrix}, \quad (57)$$

whose singular value decomposition can be used to identify dominant signal components in the discrete time series $\phi[i]$ [13]. More generally, the scalar time series $\phi[i]$ can be replaced with a vector time series of phase field values at different 3D locations, and multichannel singular spectrum analysis can be applied to identify dominant vector signal components in the time series.

Realistically, crack phase field values are not measured at individual points in a laboratory sample or the lithosphere, but may be inferred from changes in local earthquake coda wave signals. Therefore, it is noted that single/multi-channel singular spectrum analysis allows for replacement of the scalar/vector time series of crack phase field measurements $\phi[i]$ with a scalar/vector time series $\Phi[i]$ of experimentally observed data, such as relative changes in average S-wave velocity between seismic station pairs measured by monitoring coda wave signals [14]. It is conjectured that each $\Phi[i]$ is the measurement of an observable on a nonlinear dynamical system with a finite dimensional phase space \mathcal{M} , whereby the rows of the trajectory matrix $\mathcal{X}(\Phi[i])$ provide an embedding of the phase space trajectory in \mathcal{M} into \mathbb{R}^n . Based on this conjecture, an estimate of the dimension of the phase space trajectory in \mathcal{M} is provided by computing the correlation dimension of the phase space trajectory embedded in \mathbb{R}^n .

The conjectured existence of a finite dimensional nonlinear dynamical system describing time evolution of the fault damage zone is a generalization of a previous claim by seismologists that the average damage along an earthquake fault preceding its rupture evolves according to a 1 dimensional nonlinear dynamical system [15]. From this point of view, if the damage field can be decomposed into a linear superposition of finitely many time independent damage modes $\phi_i(x, y, z)$ with time dependent coefficients $a_i(\tau)$:

$$\phi(x, y, z, \tau) = \sum_{i=1}^m a_i(\tau) \phi_i(x, y, z), \quad (58)$$

a nonlinear dynamical system:

$$\begin{aligned} \frac{da_1}{d\tau} &= F_1(a_1, a_2, \dots, a_m) \\ \frac{da_2}{d\tau} &= F_2(a_1, a_2, \dots, a_m) \\ &\vdots \\ \frac{da_m}{d\tau} &= F_m(a_1, a_2, \dots, a_m) \end{aligned} \quad (59)$$

specifies time evolution of the phase field and \mathcal{M} is contained in \mathbb{R}^m . So that

each damage mode is associated with localization of strain in the lithosphere, it is further conjectured that each damage modes corresponds to a nodal displacement eigenvector of an elasto-plastic stiffness matrix $K_T^{ep}(\tau)$ with complex eigenvalue $\beta_i(\tau)$ satisfying $|\beta_i(\tau)| \ll 1$. Whether or not there is good reason to identify the eigenvalues $\beta_1(\tau), \beta_2(\tau), \dots, \beta_m(\tau)$ as branch points of a cover of the complex plane by a τ -dependent Riemann surface remains unclear.

5. Conclusion

Further computational and experimental effort is required to distinguish fundamental models of crack growth based on applied mathematics from those based on mathematical concoction. In particular, an example of simulating crack phase field time evolution in a laboratory rock sample and using singular spectrum analysis to characterize this time evolution should be provided to clarify what dynamical system governs damage time evolution. If the results of an initial computational investigation are promising, an example of using singular spectrum analysis of coda wave data to specify a finite dimensional nonlinear dynamical system should be provided as evidence for real world applicability of the signal processing method. Theoretically, to the point of providing deterministic or probabilistic analytic models of phase field time evolution, it may be useful to investigate if time evolution of an elasto-plastic tangent stiffness matrix eigenvalue distribution can be cast in terms of statistical mechanics of a 2D Coulomb gas [16].

Acknowledgements

Thanks to my family for their support during the completion of this research.

Conflicts of Interest

The author declares no conflicts of interest regarding the publication of this paper.

References

- [1] Freund, L.B. (1998) Dynamic Fracture Mechanics. Cambridge University Press.
- [2] Rice, J.R. and Simons, D.A. (1976) The Stabilization of Spreading Shear Faults by Coupled Deformation-Diffusion Effects in Fluid-Infiltrated Porous Materials. *Journal of Geophysical Research*, **81**, 5322-5334. <https://doi.org/10.1029/jb081i029p05322>
- [3] Griffiths, P. and Harris, J. (1978) Principles of Algebraic Geometry. John Wiley and Sons.
- [4] Kuhn, C. and Müller, R. (2008) A Phase Field Model for Fracture. *PAMM*, **8**, 10223-10224. <https://doi.org/10.1002/pamm.200810223>
- [5] Vermeer, P.A. and de Borst, R. (1984) Non-Associated Plasticity for Soil, Concrete and Rocks, *Heron Journal*, **29**, 1-64.
- [6] Behn, M.D., Lin, J. and Zuber, M.T. (2002) A Continuum Mechanics Model for Normal Faulting Using a Strain-Rate Softening Rheology: Implications for Thermal and Rheological Controls on Continental and Oceanic Rifting. *Earth and Planetary Science Letters*, **202**, 725-740. [https://doi.org/10.1016/s0012-821x\(02\)00792-6](https://doi.org/10.1016/s0012-821x(02)00792-6)

-
- [7] Carlson, J.M., Langer, J.S. and Shaw, B.E. (1994) Dynamics of Earthquake Faults. *Reviews of Modern Physics*, **66**, 657-670. <https://doi.org/10.1103/revmodphys.66.657>
- [8] Bindel, D.S. (2006) Structured and Parameter-Dependent Eigensolvers for Simulation-Based Design of Resonant MEMS. Ph.D. Thesis, University of California.
- [9] Aki, K. (1985) Theory of Earthquake Prediction with Special Reference to Monitoring of the Quality Factor of Lithosphere by the Coda Method. In: Kisslinger, C. and Rikitake, T., Eds., *Practical Approaches to Earthquake Prediction and Warning*, Springer, 219-230. https://doi.org/10.1007/978-94-017-2738-9_2
- [10] Wu, R. and Aki, K. (1985) The Fractal Nature of the Inhomogeneities in the Lithosphere Evidenced from Seismic Wave Scattering. *Pure and Applied Geophysics*, **123**, 805-818. <https://doi.org/10.1007/bf00876971>
- [11] Sato, H. (2019) Power Spectra of Random Heterogeneities in the Solid Earth. *Solid Earth*, **10**, 275-292. <https://doi.org/10.5194/se-10-275-2019>
- [12] Lyakhovsky, V., Ben-Zion, Y. and Agnon, A. (1997) Distributed Damage, Faulting, and Friction. *Journal of Geophysical Research: Solid Earth*, **102**, 27635-27649. <https://doi.org/10.1029/97jb01896>
- [13] Broomhead, D.S. and King, G.P. (1986) Extracting Qualitative Dynamics from Experimental Data. *Physica D: Nonlinear Phenomena*, **20**, 217-236. [https://doi.org/10.1016/0167-2789\(86\)90031-x](https://doi.org/10.1016/0167-2789(86)90031-x)
- [14] Merrill, R.J., Bostock, M.G., Peacock, S.M. and Chapman, D.S. (2023) Optimal Multichannel Stretch Factors for Estimating Changes in Seismic Velocity: Application to the 2012 mw 7.8 Haida Gwaii Earthquake. *Bulletin of the Seismological Society of America*, **113**, 1077-1090. <https://doi.org/10.1785/0120220250>
- [15] Ben-Zion, Y. and Lyakhovsky, V. (2002) Accelerated Seismic Release and Related Aspects of Seismicity Patterns on Earthquake Faults. *Pure and Applied Geophysics*, **159**, 2385-2412. <https://doi.org/10.1007/s00024-002-8740-9>
- [16] Saleur, H., Sammis, C.G. and Sornette, D. (1996) Renormalization Group Theory of Earthquakes. *Nonlinear Processes in Geophysics*, **3**, 102-109. <https://doi.org/10.5194/npg-3-102-1996>